

# SCIENTIFIC REPORTS

OPEN

## Eutectic modification by ternary compound cluster formation in Al-Si alloys

J. Barrirero<sup>1,2</sup>, C. Pauly<sup>1</sup>, M. Engstler<sup>1</sup>, J. Ghanbaja<sup>3</sup>, N. Ghafoor<sup>2</sup>, J. Li<sup>4</sup>, P. Schumacher<sup>4</sup>, M. Odén<sup>2</sup> & F. Mücklich<sup>1</sup>

Al-alloys with Si as the main alloying element constitute the vast majority of Al castings used commercially today. The eutectic Si microstructure in these alloys can be modified from plate-like to coral-like by the addition of a small amount of a third element to improve ductility and toughness. In this investigation the effects of Eu and Yb are studied and their influence on the microstructure is compared to further understand this modification. The two elements impact the alloy differently, where Eu modifies Si into a coral-like structure while Yb does not. Atom probe tomography shows that Eu is present within the Si phase in the form of ternary compound  $\text{Al}_2\text{Si}_2\text{Eu}$  clusters, while Yb is absent in the Si phase. This indicates that the presence of ternary compound clusters within Si is a necessary condition for the formation of a coral-like structure. A crystallographic orientation relationship between Si and the  $\text{Al}_2\text{Si}_2\text{Eu}$  phase was found, where the following plane normals are parallel:  $011_{\text{Si}}//0001_{\text{Al}_2\text{Si}_2\text{Eu}}$ ,  $111_{\text{Si}}//6710_{\text{Al}_2\text{Si}_2\text{Eu}}$  and  $011_{\text{Si}}//6710_{\text{Al}_2\text{Si}_2\text{Eu}}$ . No crystallographic relationship was found between Si and  $\text{Al}_2\text{Si}_2\text{Yb}$ . The heterogeneous formation of coherent  $\text{Al}_2\text{Si}_2\text{Eu}$  clusters inside the Si-phase is suggested to trigger the modification of the microstructure.

The use of light-weight castings in the automotive sector results in higher energy efficiency and reduced fuel consumption. Al-Si alloys are frequently used for such castings because of their excellent fluidity, castability, and corrosion resistance<sup>1</sup>. Al-Si alloys have an irregular eutectic phase with faceted Si plates in a non-faceted aluminium matrix. The Si plates act as crack propagation paths that deteriorate the ductility and toughness of the material<sup>2,3</sup>. To improve these properties, the Si plate-like morphology is modified to a coral-like microstructure<sup>4,5</sup>. Small amounts of certain elements such as Na, Sr, or Eu are added to the alloy to completely change the Si-plates to finer, rounded coral branches. The reduced size and geometric aspect ratio of the modified eutectic enhances the toughness of the alloy by reducing the local stress concentrations such that crack initiation is suppressed and crack propagation resistance is increased<sup>3,6,7</sup>. The secondary dendrite arm spacing (SDAS) of the Si-phase is affected by the cooling rate during casting and by combining appropriate casting conditions with additions of modifier and grain refiner, significant improvements in tensile<sup>8-10</sup> and impact properties<sup>2,6,11</sup> are obtained.

Understanding the exact underlying mechanism for this remarkable change in structure has been an outstanding research topic ever since the discovery of the modification, almost 100 years ago<sup>12</sup> and the interaction between Al, Si, and the modifying agents is not yet fully elucidated. Without such knowledge it is impossible to control the homogeneity of the modification for more complex alloys such as Al-Si-Mg and Al-Si-Mg-Cu.

Several studies have considered the effect of the modifier during nucleation and growth of the eutectic phase<sup>13-19</sup>. One of the most distinctive characteristics of the modified Si-phase is the large amount of crystallographic defects<sup>17,20,21</sup>. A well accepted hypothesis by Lu and Hellawell<sup>19</sup> for the multiplication of defects is the so called impurity induced twinning (IIT). They proposed poisoning of step sources across the closely packed {111} planes in Si by the adsorption of atoms of the modifying agent at the solidification front. They formulated a geometric model to predict the optimal ratio between the atomic radius of the modifying agent and Si such that the adsorption of this impurity on a {111}<sub>Si</sub> step would cause a displacement resulting in a different stacking sequence and

<sup>1</sup>Functional Materials, Department of Materials Science, Saarland University, D-66123, Saarbrücken, Germany.

<sup>2</sup>Nanostructured Materials, Department of Physics, Chemistry and Biology (IFM), Linköping University, SE-58183, Linköping, Sweden. <sup>3</sup>Institut Jean Lamour, UMR CNRS 7198, Université de Lorraine, F-54042, Nancy, France.

<sup>4</sup>Institute of Casting Research, Montanuniversität Leoben, A-8700, Leoben, Austria. Correspondence and requests for materials should be addressed to J.B. (email: [j.barrirero@mx.uni-saarland.de](mailto:j.barrirero@mx.uni-saarland.de))

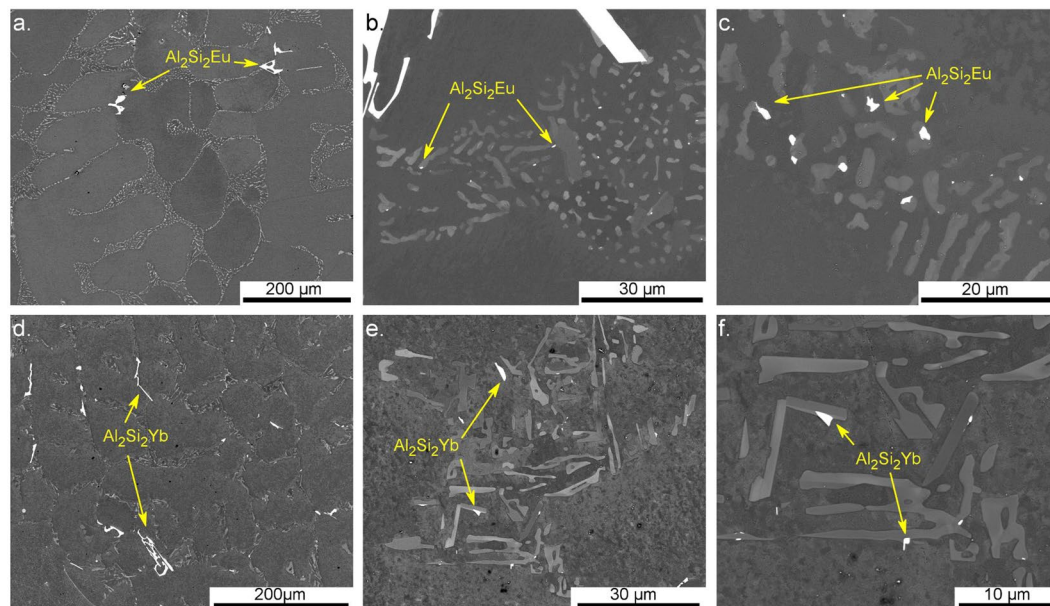


**Figure 1.** SEM micrographs of Al-5 wt.%Si with either Eu (a–c) or Yb (d–f) additions. (a) Coral-like eutectic phase and pre-eutectic coarse  $\text{Al}_2\text{Si}_2\text{Eu}$  intermetallics; (b,c) smaller  $\text{Al}_2\text{Si}_2\text{Eu}$  intermetallic phases formed during eutectic growth. (d) Refined structure resembling the plate-like eutectic phase of unmodified alloys and coarse  $\text{Al}_2\text{Si}_2\text{Yb}$  intermetallics; (e,f) smaller intermetallic phases forming during eutectic growth.

promoting frequent twinning. According to this model the optimal atomic radius of the modifying agent should be 1.65 times larger than the one of Si.

Based on the IIT-model, several elements other than the well-known Na and Sr have been tested as possible alloy modifiers<sup>22–24</sup>. Nogita *et al.*<sup>24</sup>, studied the microstructure of the eutectic phase after addition of almost all rare earth metals and found that, although all of them caused suppressed eutectic growth temperature, the only element able to form the coral-like structure was europium (Eu). In fact, ytterbium (Yb), which is the element with the best fit to the IIT-model ( $r_{\text{Yb}}/r_{\text{Si}} = 1.66$ ) shows, similar to many other rare earth metals, only a refinement of the Si plate-like structure. This shows that the atomic radius alone is not capable of predicting the morphological transition of the eutectic structure and the reason why they behave differently remains an open question.

Recent studies using atom probe tomography (APT) with the possibility of obtaining spatially resolved chemical information from crystallographic defects in the Si-phase have shown co-segregation of Al atoms and the modifier agent in alloys modified with Sr and Na<sup>25–28</sup>. The defects showed chemical compositions consistent with  $\text{Al}_2\text{Si}_2\text{Sr}$  and  $\text{AlSiNa}$ <sup>26</sup>. Based on this, the formation of the coral-like Si structure was proposed to be related to the formation of clusters of ternary compounds at the solidification front rather than the adsorption of single atoms.

The present study investigates and compares the effect of Eu and Yb additions on the microstructure of an Al-Si alloy at different length scales. The aim is to confirm whether the formation of ternary compounds plays a role during the growth of Si corals by Eu addition and highlight the difference of the Si crystal growth with the addition of elements that only refine the Si plate structure such as Yb. Li *et al.*<sup>29</sup> have shown the presence of Eu at crystallographic defects in the Si phase by high resolution scanning transmission electron microscopy (STEM). The difficulty faced with this technique is that Al atoms in the Si lattice cannot be identified due to the small difference in atomic weight between Al and Si. They also used electron energy loss spectroscopy (EELS) to determine the distribution of Eu atoms within Si but were not able to chemically resolve Al atoms present in the Si crystal. To overcome this problem we used APT, which offers the possibility to study and compare the three-dimensional distribution of Al, Eu and Yb in the Si phase. Transmission electron microscopy (TEM), electron back-scattered diffraction (EBSD), transmission Kikuchi diffraction (TKD) and back-scattered electron (BSE) imaging are also used as complementary techniques to compare the eutectic microstructures at different length scales and to study the orientation relationship between the phases.

## Results

Figure 1 shows two distinct microstructures when adding 0.05 wt.% Eu (Fig. 1(a–c)) or 0.61 wt.% Yb (Fig. 1(d–f)) to an Al-5 wt.% Si alloy. Eu addition results in a homogeneously modified coral-like Si structure, while Yb addition shows less drastic morphological change with a coarser microstructure similar to the plate-like structure of the unmodified alloys. Several studies report that Yb acts just as a refiner of the unmodified plate-like structure<sup>22,24,30,31</sup>. Our results show a mixed structure with straight elongated Si-branches similar to plates together with more rounded ones.

The regions giving bright contrast by backscattered electrons on the polished surfaces are  $\text{Al}_2\text{Si}_2\text{Eu}$  and  $\text{Al}_2\text{Si}_2\text{Yb}$  intermetallic phases. The presence of the intermetallic compounds was confirmed by standardless quantitative EDS and their EBSD Kikuchi patterns were successfully indexed to match the crystallographic structure

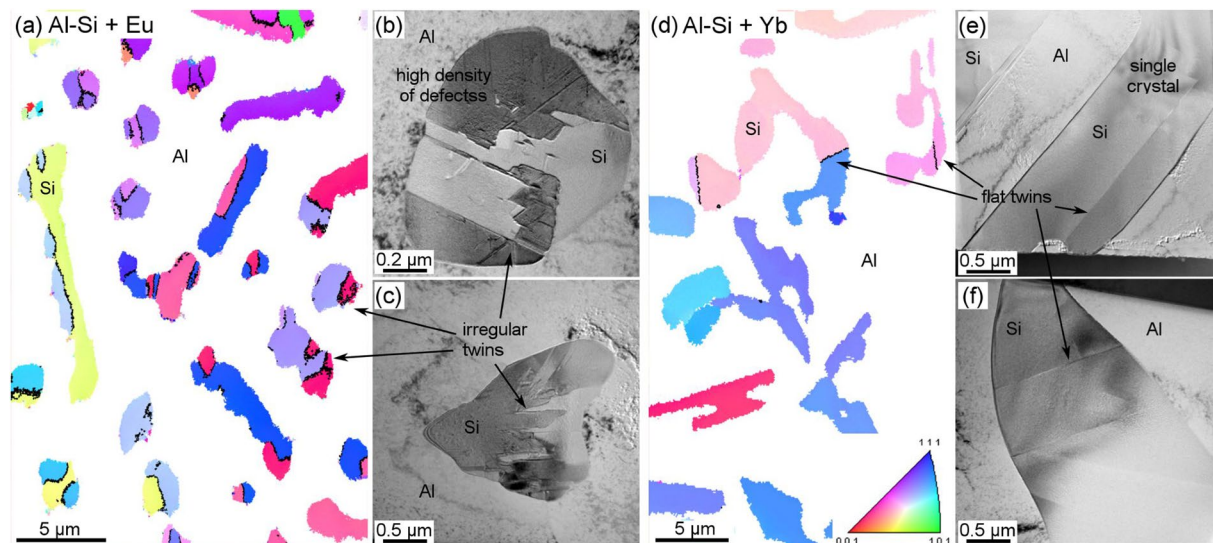


**Figure 2.** Inverse pole figures of EBSD maps in Al-5 wt.%Si alloys modified by: (a) Eu (step size 30 nm) and (d) Yb (step size 90 nm). Black lines show twin boundaries in Si. White areas correspond to the Al matrix which was filtered out for clarity. TEM images show high density of crystallographic defects in the Si structure of the Eu modified alloy (b,c); and only flat twin planes across the Si crystal in the alloy with Yb addition (e,f).

of  $\text{Al}_2\text{Si}_2\text{Eu}$  and  $\text{Al}_2\text{Si}_2\text{Yb}$ , respectively<sup>32–34</sup>. Figure 1 shows how these ternary compound particles are present with two different sizes. In Fig. 1(a,d), coarse (tens of micrometres) pre-eutectic intermetallic particles are present, while Fig. 1(b,c,e,f) show particles formed during eutectic solidification with sizes ranging from sub-micrometre to a few micrometres.

Figure 2 shows the difference between the eutectic Si structures of the two alloys investigated. Black lines in the EBSD images (Fig. 2(a,d)) highlight irregular  $\Sigma 3$  twin boundaries for Eu addition, which is similar to that in Sr modified alloys<sup>25</sup>. Yb addition shows a lower density of twins in coarser Si branches. The EBSD map in Fig. 2(d) confirms that twin boundaries are straight, which is similar to what have been seen in the unmodified alloy<sup>25</sup>.

The TEM micrographs in Fig. 2 show the crystallographic structure of Si. All micrographs were recorded along the  $\text{Si}\langle 011 \rangle$  zone axis in order to have edge-on alignment of defects on  $\{111\}$  planes. Figure 2(b,c) shows a high density of nanotwins or stacking faults (SF) and v-shaped defects in the alloy with Eu addition, which is consistent with what has been reported for Sr and Na modifications<sup>25,26</sup>. Moreover, the boundaries between the areas with different contrast in the Si phase show irregular shaped twin boundaries. The alloy with Yb addition presents only straight twins through the crystal (Fig. 2(e,f)).

APT reconstructions in Fig. 3 display differences in the solutes' distribution in the two alloys. The alloy with Eu addition contains clusters of Eu and Al in the Si structure. Similar to Sr and Na modified alloys<sup>25,26</sup>, solute clusters with three different morphologies are distinguished: rod-like, planar, and rounded (Fig. 3(a)). No clusters containing only Eu or only Al could be found in the Si phase and instead Al and Eu atoms always appear together. Figure 3(b) shows an inset of one such planar cluster of solute atoms with a quantitative one-dimensional concentration profile through the cluster showing the spatial distribution of the atoms. In contrast, no rod-like or planar clusters were found in the alloy with Yb addition (Fig. 3(c)). In fact, no traces of Yb could be detected in the Si phase, i.e. Yb was not even found as solid solution in the Si-crystals. The rounded clusters found in this alloy contain Al and Si, and most of them have a core-shell structure, similar to the unmodified alloy<sup>25</sup>.

To determine the composition of the ternary compound clusters formed in the Eu modified alloy, each single rod-like and planar cluster present in three different APT specimens were isolated in tightly fitted regions of interest (ROIs) and the number of Al and Eu atoms was counted after optimization of the mass spectrum and background subtraction, following the procedure outlined in<sup>26</sup>. The details of a rod-like cluster are shown in Fig. 4(d), and the measured Al:Eu ratios for 35 rod-like and 4 planar clusters are plotted in Fig. 4(e). The average Al:Eu ratio for all these clusters is  $2.25 \pm 0.42$ . When considering 2–5 nanometre thick clusters, the atomic positions in APT can be influenced by ion trajectory overlaps due to local magnification effects<sup>35</sup>. This artefact may lead to a convolution of the matrix, in this case Si, with the cluster resulting in an overestimation of the matrix element<sup>35–39</sup>. Given this uncertainty, it is not possible to discriminate between the “matrix Si” and Si in the cluster. Because of this reason, only Al and Eu atoms are considered and reporting relative solute ratios Al:Eu is more adequate than absolute concentrations in the clusters.

Figure 4(a,b,c) shows three perspectives of one APT specimen with a high density of rod-like clusters. All rounded clusters and dissolved solutes in the specimen were masked out to reveal the structure of the rod-like defects. In Fig. 4(a), the specimen is oriented to display the v-shape character of the defects in a similar way to how they are seen by TEM. Figure 4(b,c) are obtained by rotating the specimen. These images reveal the three-dimensional structure of the crystallographic defects in the Si lattice and show how misleading the two-dimensional projection obtained by TEM can be. In several occasions, what we see and denote as v-shaped

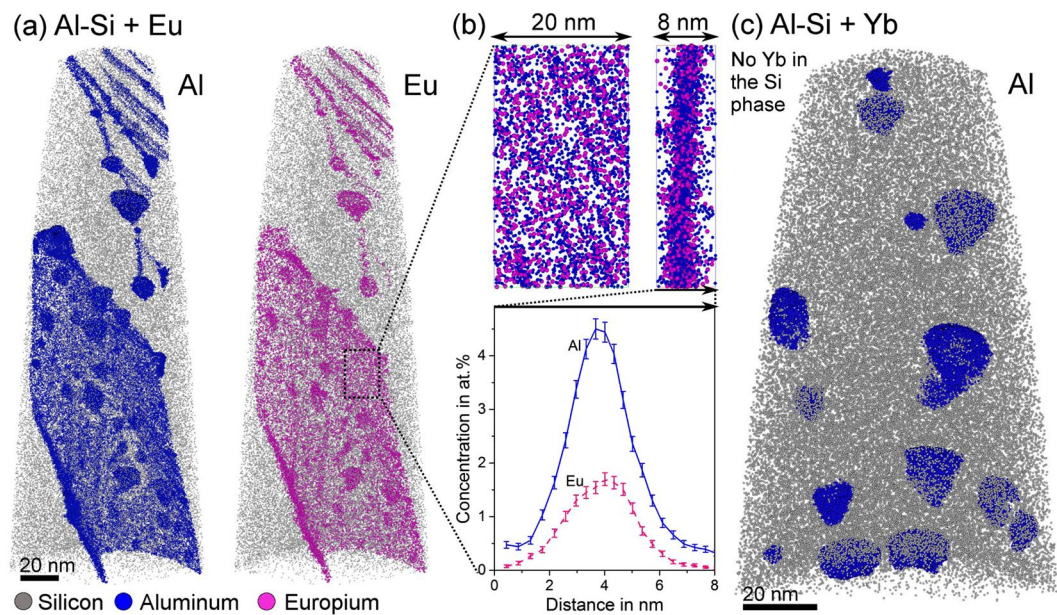


**Figure 3.** APT comparison of the solute distribution in Si. (a) Alloy modified by Eu presenting rod-like, planar and round clusters, all of them containing Al and Eu; (b) inset of the planar atomic clustering with a one-dimensional concentration profile across the segregation plane. (c) Alloy with Yb addition presenting only Al rounded clusters in Si. No Yb peaks were detected in the mass spectrum of the Si phase.

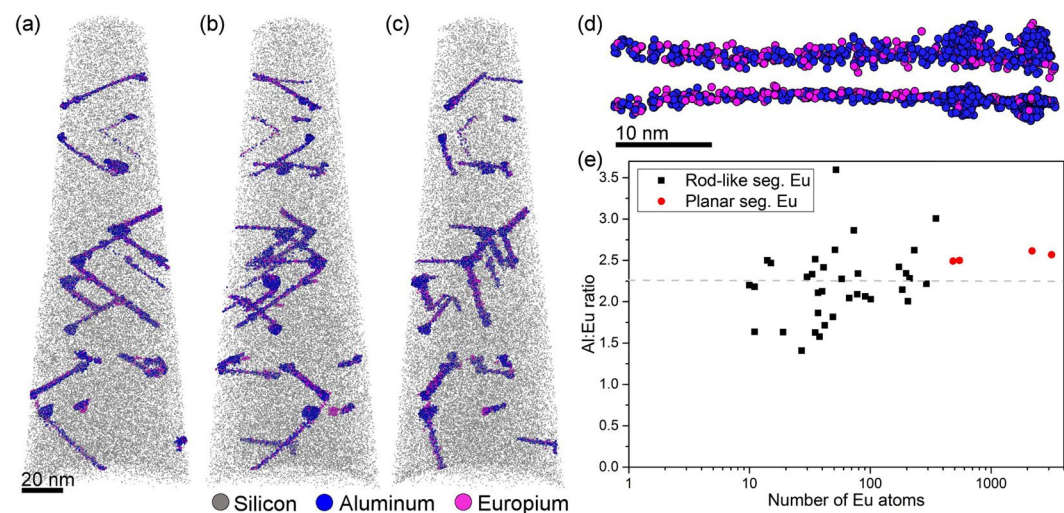


**Figure 4.** APT analysis of eutectic Si. (a), (b), and (c) are views of the same specimen at different rotation angles showing the scaffold of rod-like segregations in the Si lattice. (d) Shows one isolated rod-like segregation viewed from the top and the side. (e) Al:Eu ratios as a function of the number of Eu atoms in each of the 39 clusters (35 rod-like and 4 planar).

defects are actually three rod-like clusters originating from one point or two different clusters positioned at different planes in space. Instead of v-shaped defects, APT shows a complex three-dimensional structure of the crystallographic defects in Si. For clarity, videos are included as supplementary material to get complete 3D-views (Supplementary Video S1 and S2).

APT specimens of eutectic Al were analysed and no traces of Eu and Yb were detected with a detection limit of 50 at. ppm showing a negligible solubility of these elements in Al.

The crystallographic orientations between Si and the micrometre sized eutectic  $\text{Al}_2\text{Si}_2\text{Eu}$  or  $\text{Al}_2\text{Si}_2\text{Yb}$  phases were analysed by EBSD and TKD. For this analysis, 17 different Si/ $\text{Al}_2\text{Si}_2\text{Eu}$  boundaries and 10 Si/ $\text{Al}_2\text{Si}_2\text{Yb}$  boundaries were scanned. Pole figures of the low index plane-normals 001, 011 and 111 in Si were constructed and compared with the pole figures of the low index plane-normals 0001,  $11\bar{2}0$ ,  $01\bar{2}2$  and  $11\bar{2}1$  in  $\text{Al}_2\text{Si}_2\text{X}$  (X = Eu, Yb). This comparison allows looking for crystallographic orientation relationships between the ternary phases and the Si crystal. The spatial coincidences of poles from the two phases show parallel plane-normals, or

what is the same, parallel planes of the two phases. Alloys modified by Eu showed coincidence of  $011_{\text{Si}}$  and  $0001_{\text{Al}_2\text{Si}_2\text{Eu}}$  poles in 15 out of the 17 cases analysed, while the alloy with Yb addition only showed this orientation relationship in 2 out of 10 cases.

TKD/EBSD datasets were then rotated to have the  $0001_{\text{Al}_2\text{Si}_2\text{Eu}}$  plane-normal at the centre of the pole figure, i.e. at the normal direction (ND), to find a further orientation relationship perpendicular to the  $(0001)_{\text{Al}_2\text{Si}_2\text{Eu}}$  lattice plane. Two mutually perpendicular orientation relationships between the crystals define a fixed three-dimensional orientation relationship. Figure 5 shows an example of three Si crystals next to an  $\text{Al}_2\text{Si}_2\text{Eu}$  phase which fulfil the  $011_{\text{Si}}//0001_{\text{Al}_2\text{Si}_2\text{Eu}}$  orientation relationship (Fig. 5(b,c,d,e)). In this condition, pole coincidences depicting parallel plane-normals between the low index  $\{011\}$ ,  $\{111\}$  Si plane-families and the  $\{6\bar{7}10\}$   $\text{Al}_2\text{Si}_2\text{Eu}$  plane-family were determined (Fig. 5(c,d,e)). The simultaneous orientation relationships  $011_{\text{Si}}//0001_{\text{Al}_2\text{Si}_2\text{Eu}}$  and  $111_{\text{Si}}//6\bar{7}10_{\text{Al}_2\text{Si}_2\text{Eu}}$  or  $011_{\text{Si}}//6\bar{7}10_{\text{Al}_2\text{Si}_2\text{Eu}}$  describe a fixed growth orientation between Si and  $\text{Al}_2\text{Si}_2\text{Eu}$  which is not present in the case of Si and  $\text{Al}_2\text{Si}_2\text{Yb}$ .

The three Si crystals shown in Fig. 5 are mutually related by coherent twin boundaries  $\Sigma 3$  and the special grain boundary  $\Sigma 9$  (marked in black and green in Fig. 5(b), respectively). We note that all three Si grain-orientations have parallel low index planes to some plane in the  $\{6\bar{7}10\}$  family of the same  $\text{Al}_2\text{Si}_2\text{Eu}$  grain.  $(6\bar{7}10)_{\text{Al}_2\text{Si}_2\text{Eu}}$  plane deviates  $7.6^\circ$  from the low index plane  $(1\bar{1}00)_{\text{Al}_2\text{Si}_2\text{Eu}}$ .

The misfits of the interplanar spacings between Si and  $\text{Al}_2\text{Si}_2\text{Eu}$  were calculated to prove the feasibility of a coherent growth of the phases in the orientations found in the pole figures. Table 1 shows misfits smaller than 6% between multiples of the d-spacings. Several other pole coincidences were found involving the Si low index planes and  $\text{Al}_2\text{Si}_2\text{Eu}$   $\{12\bar{3}0\}$ ,  $\{1\bar{1}00\}$  and  $\{1\bar{1}03\}$  plane-families. Not all coincidences are shown in Fig. 5 for clarity. The relationship between the two mutually perpendicular sets of planes in both lattices is enough to describe the fixed orientation relationship between the crystals.

## Discussion

The addition of eutectic modifiers in Al-Si castings affects solidification in several aspects. Eutectic nucleation sites are poisoned causing a depression of the nucleation and growth temperatures, and a strong decrease in the density of eutectic grains<sup>15,40–46</sup>. Fewer and larger grains have a smaller total solid/liquid surface area. To account for a given cooling rate the modified eutectic phase solidifies with a higher interface velocity and, therefore, the microstructure inside the eutectic grains is refined<sup>13,14</sup>. However, the plate-to-coral morphology transition of Si was shown to be independent of alterations in nucleation mode and frequency<sup>47</sup>. The morphology transformation is rather a consequence of an additional effect of the modifier during Si growth. A significant increase of crystallographic defects in Si has been explained by the poisoning of re-entrant twins' edges<sup>48–52</sup> and by the impurity induced twinning (IIT) model<sup>19</sup>. The latter points out several atomic species as potential eutectic modifiers of Al-Si alloys<sup>19</sup>. This theory is based on single atoms modifying the structure by poisoning preferred growth orientations. The poisoning atom should optimally be 1.65 times larger than the Si-atom, which would interrupt the growth such that one monolayer in the regular close packed plane stacking sequence is skipped and instead a twin is formed.

Today we know that, although the modifier agent influences the formation of crystallographic defects, the atomic radius itself cannot be taken as an indication of potency of modification. This is exemplified as just some of the elements proposed in IIT form Si-corals. For example, Yb has the ideal ratio  $r_{\text{Si}}/r_{\text{Yb}} = 1.65$  but it only refines the plate-like Si structure<sup>22,30,31</sup>, while Eu having a ratio of 1.72 is as potent as Na and Sr to form Si-corals<sup>30,53</sup>. Further, in this paper we show that an efficient modifier like Eu always appears together with Al in the defects of the Si lattice (Figs 3 and 4) and never as single atoms. This is in accordance with other efficient modifiers such as Sr and Na, which showed compositions inside the defects consistent with  $\text{Al}_2\text{Si}_2\text{Sr}$  and  $\text{AlSiNa}$ <sup>25,26</sup>. In the present work, the average Al:Eu ratio of nearly 2 (Fig. 4(e)) suggests that the ternary compound  $\text{Al}_2\text{Si}_2\text{Eu}$  is formed at the defects and in this case the geometric IIT model is no longer valid. The presence of clusters of  $\text{Al}_2\text{Si}_2\text{Eu}$  at the defects in the Si lattice stresses the importance of atomic interaction between Si, the third element (in this case Eu), and Al during solidification.

The formation of the eutectic ternary compounds  $\text{Al}_2\text{Si}_2\text{Eu}$  and  $\text{Al}_2\text{Si}_2\text{Yb}$  (Figs 1(b,c,e,f); 5(a)) indicates that there is sufficient driving force for nucleation and growth of these phases during solidification. To the best of our knowledge, the liquidus surfaces for Al-Si-Eu and Al-Si-Yb ternary systems are not known. However, the liquidus surfaces for alloys with other modifiers such as Al-Si-Sr<sup>54</sup>, Al-Si-Na<sup>55</sup> and Al-Si-Ca<sup>56</sup> show a ternary eutectic point close to the temperature and composition of the binary Al-Si and at low amounts of Sr (0.03 at.%), Na (0.01 at.%), or Ca (0.7 at.%). Based on the back-scattered-electron images in Fig. 1 and other studies<sup>29–31,53</sup>, it is reasonable to assume that Al-Si-Eu and Al-Si-Yb alloys also present such eutectic point. At the ternary eutectic point, three phases are expected: Al, Si, and a ternary compound inherent to each system.

Examining the ternary eutectic solidification path and keeping in mind that the amount of the third element (Eu, Yb) in the alloy is low, there is a simultaneous solidification of the two major phases (Al and Si) during the entire eutectic reaction. The third phase will only form when the third element's local concentration is high enough. APT results show that almost no Eu or Yb is dissolved in the eutectic Al or Si. Instead, these elements are expected to be accumulated ahead of the solidification front resulting in a concentration gradient of Eu or Yb perpendicular to the growth front. Such accumulation of the modifying element has been proposed in several studies<sup>50,57–59</sup> and it gives the necessary conditions of constitutional undercooling and supersaturation for ternary compounds to form. The Gibbs free energy for nucleation of embryos is a function of the undercooling and the local supersaturation of the elements. At the eutectic temperature, the diffusion boundary layer at the solid/liquid interface has an increased amount of the third element causing the melt to locally be more undercooled<sup>22,31,53</sup>. Under these conditions, sub-critical clusters (embryos) of the ternary phase will form and re-melt in the liquid until there is enough supersaturation for a cluster to reach a critical size and grow to a micrometre-sized grain as

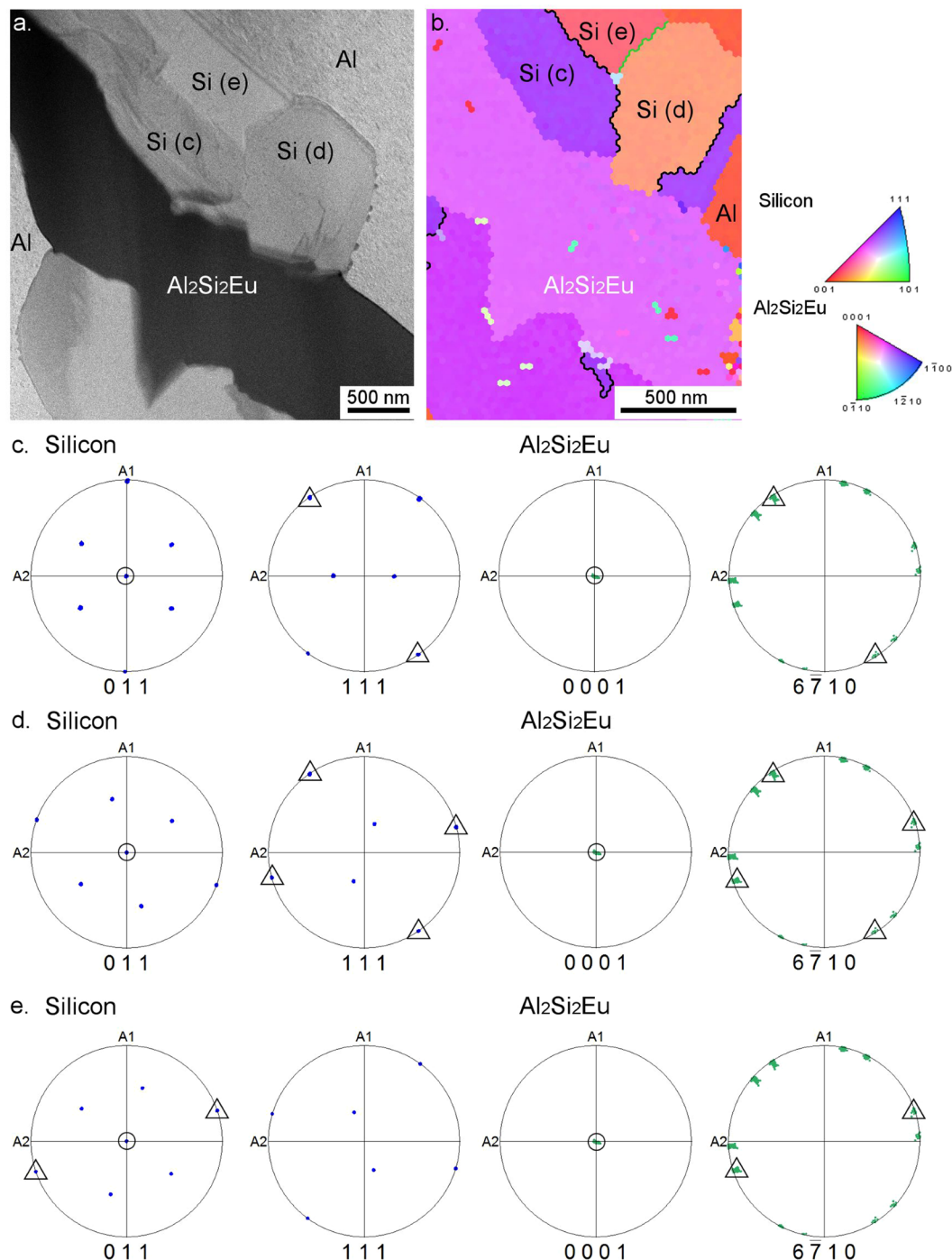


**Figure 5.** Crystallographic orientation relationship between Si and eutectic  $\text{Al}_2\text{Si}_2\text{Eu}$ : **(a)** bright field TEM image showing eutectic  $\text{Al}_2\text{Si}_2\text{Eu}$  surrounded by Si; **(b)** inverse pole figure of a TKD map showing mutually twinned Si crystal orientations. Black boundaries between Si grains show  $\Sigma 3$  twin ( $60^\circ @ \langle 111 \rangle$ ), and the green boundary highlights a  $\Sigma 9$  twin ( $38.9^\circ @ \langle 110 \rangle$ ). **(c–e)** Pole figures (PF) corresponding to the three Si crystals marked in **(b)**. All PF were re-oriented to the  $(0001)_{\text{Al}_2\text{Si}_2\text{Eu}}$  in the normal direction (ND) for convenience. Circles depict coincident poles (parallel plane-normals) between  $011_{\text{Si}}$  and  $0001_{\text{Al}_2\text{Si}_2\text{Eu}}$ . Triangles depict coincident poles in  $011_{\text{Si}}$ ,  $111_{\text{Si}}$  and  $6\bar{7}10_{\text{Al}_2\text{Si}_2\text{Eu}}$ .

seen in Fig. 1(b,c,e,f). Figures 1(c,f) and 5(a) highlight how the eutectic ternary phase is formed on the Si phase and do not grow independently or as a part of eutectic Al. This observation emphasizes that these phases are most probably heterogeneously nucleated at the Si interface. This is reasonable because the  $\text{Al}_2\text{Si}_2\text{X}$  phases normally have an ordered hexagonal structure (space group  $P-3m1$  (164)) and grow in a faceted manner such as Si. This tendency towards faceted growth can be seen in the polyhedral morphology of the pre-eutectic coarse particles (Fig. 1(a,d)).

d-Spacings and multiples (nm)		Misfit $\delta$ (%)
	d- $\{6\bar{7}10\}_{Al_2Si_2Eu} = 0.0552$	
d- $\{111\}_{Si} = 0.314$	$(6 \times) d-\{6\bar{7}10\} = 0.331$	-5.19
d- $\{011\}_{Si} = 0.384$	$(7 \times) d-\{6\bar{7}10\} = 0.386$	0.62
	<b>d-<math>\{011\}_{Si} = 0.384</math></b>	
d- $\{0001\}_{Al_2Si_2Eu} = 0.726$	$(2 \times) d-\{011\}_{Si} = 0.768$	-5.79

**Table 1.** Misfits of  $Al_2Si_2Eu$  related to Si for the parallel planes found in EBSD/TKD.

	Space group	Lattice parameters		d-spacing (nm)	Misfit $\delta$ %	Si structure
		a,b (nm)	c (nm)			
Si	Fd-3m (227)	0.543	0.543	d(110) = 0.384	—	—
$Al_2Si_2Sr$ <sup>63</sup>	P-3m1 (164)	0.418	0.743	d(0002) = 0.372	-3.36	Coral
$AlSiNa$ <sup>64</sup>	P4/nmmO2 (129)	0.414	0.738	d(002) = 0.369	-4.07	Coral
$Al_2Si_2Eu$ <sup>33</sup>	<b>P-3m1 (164)</b>	<b>0.418</b>	<b>0.726</b>	<b>d(0002) = 0.363</b>	<b>-5.79</b>	<b>Coral</b>
$Al_2Si_2Ca$ <sup>63</sup>	P-3m1 (164)	0.413	0.715	d(0002) = 0.358	-7.41	Mixed
$Al_2Si_2Ba$ <sup>65</sup>	I4/mmm (139)	0.423	0.698	d(0002) = 0.349	-10.03	Mixed
$Al_2Si_2Yb$ <sup>33</sup>	<b>P-3m1 (164)</b>	<b>0.414</b>	<b>0.695</b>	<b>d(0002) = 0.348</b>	<b>-10.50</b>	<b>Refined plates</b>
$Al_2Si_2Y$ <sup>66</sup>	P-3m1 (164)	0.418	0.656	d(0002) = 0.328	-17.07	Refined plates

**Table 2.** Crystal structure and misfit of ternary compounds related to Si.

The microstructural comparison between the two alloys studied here shows that they have similar solidification paths. Both alloys have a ternary eutectic point with formation of  $Al_2Si_2X$  (Eu, Yb) (Fig. 1). The difference between the two alloys is Eu's ability to form early stage  $Al_2Si_2Eu$  clusters on the facets of the Si crystal, while such clusters are absent in the alloy containing Yb (Figs 3 and 4). The formation of clusters on the Si-facets during solidification affects the Si-growth by local obstruction, causing steps on the facets and increasing growth direction diversity. This growth restriction model is different to the IIT model, as it incorporates the much larger ternary clusters as growth obstacle on the Si surfaces explaining more readily the high density of crystallographic defects in Si and the modification from Si plates to corals.

We postulate that the difference between the effect of Eu and Yb stems from the difference in the energy needed for sub-critical clusters of  $Al_2Si_2Eu$  and  $Al_2Si_2Yb$  to form on solidified Si surfaces. In other words,  $Al_2Si_2Eu$  clusters need less energy to form on Si in comparison to  $Al_2Si_2Yb$  clusters. The strong accumulation of the modifier together with Al and Si on the first tens of nanometres ahead of the solidification front, gives the necessary condition of constitutional undercooling and supersaturation for the ternary clusters to form. Eu and Yb atoms will be eventually trapped at the Si surface as part of ternary clusters formed heterogeneously at the interface. However, the cluster formation is only energetically favourable for a good lattice match onto the Si surface. The presence of  $Al_2Si_2Eu$  clusters showed by APT suggests a good lattice match with Si, in contrast to  $Al_2Si_2Yb$ . Although Yb atoms may sit shortly onto the Si interface, the lattice mismatch of the ternary cluster cost too much energy and dissolves or cannot form.

Direct determination of the formation energy of heterogeneous clusters of  $Al_2Si_2Eu$  and  $Al_2Si_2Yb$  on different facets of the Si crystal during eutectic solidification is challenging, both experimentally and by simulations. Instead, we have adopted an indirect approach to test our arguments by studying the crystallographic orientation relationships between Si and each of the two ternary phases. The expected crystallographic orientation relationship between fcc and hcp is the alignment of the close packed planes  $111_{fcc}/0001_{hcp}$ . However, Fig. 5 shows EBSD/TKD pole figures of  $Al_2Si_2Eu$  in contact with Si, showing unexpected parallel plane-normals:  $111_{Si}/6\bar{7}10_{Al_2Si_2Eu}$ ,  $011_{Si}/6\bar{7}10_{Al_2Si_2Eu}$  and  $011_{Si}/0001_{Al_2Si_2Eu}$  with misfits of the d-spacings smaller than 6% (Table 1). This result indicates heterogeneous formation of  $Al_2Si_2Eu$  with an epitaxial relationship to the Si surface, while such relationship is not present in the case of  $Al_2Si_2Yb$ . Both ternary compounds,  $Al_2Si_2Eu$  and  $Al_2Si_2Yb$ , have the same hexagonal P-3m1 crystal structure with a = b lattice parameters that differ less than 1%, while c differs more than 4% (Table 2). Considering the orientation relationship reported in Fig. 5, the different potency of heterogeneous nucleation for these two phases on Si is evaluated on the basis of the misfit between the Si-surface and the nucleating phases. The interplanar spacings  $d(0002)_{Al_2Si_2Eu} = 0.363$  nm and  $d(0002)_{Al_2Si_2Yb} = 0.348$  nm can be compared to  $d(110)_{Si} = 0.384$  nm. This comparison shows misfits of 5.79% for  $Al_2Si_2Eu$  and 10.50% for  $Al_2Si_2Yb$  towards Si. The higher mismatch of the Yb phase adds strain energy to its nucleation, which makes  $Al_2Si_2Yb$  clusters less stable than  $Al_2Si_2Eu$  clusters on Si facets.

This calculation can be applied to similar ternary phases present in the Al-Si alloys with addition of other elements. Table 2 shows how the three systems forming Si corals (addition of Na, Sr or Eu), have ternary phases with a misfit smaller than 6%. Ca and Ba, elements which can induce the formation of fibrous Si similar to the coral structure when higher amounts of these elements are added<sup>22,23</sup>, have a higher misfit, while Yb and Y ternary phases show the highest misfits and also the lowest potency as modifiers<sup>22,31</sup>.

The reason why clusters with a rod-like morphology are the most frequently found is likely an effect of different misfits in different orientations on the Si-surface. Such dispersion in misfit favors growth of the cluster in specific orientations. These results show a consistent difference between the elements tested as possible modifiers in literature and the degree of Si microstructural modification into corals. Li *et al.*<sup>29</sup> showed by high resolution STEM imaging how columns of Eu atoms match every second Si pair of dumbbells on a  $111_{\text{Si}}$  plane. The approximated distance between Eu columns that can be measured from their image is  $\sim 0.7$  nm, i.e. the  $c$  distance of  $\text{Al}_2\text{Si}_2\text{Eu}$ . Al and Si atoms between Eu columns cannot be differentiated in HAADF-STEM mode because of the projection of the entire thickness of the TEM sample on the image (about 20 nm with more than 20 Al and Si atomic layers) and because of the small  $Z$  difference between Al and Si. However, the distance between Eu columns can be explained by the early stage formation of atomic layers of the  $\text{Al}_2\text{Si}_2\text{Eu}$  ternary compound on a  $111_{\text{Si}}$  plane as postulated in this work.

## Conclusion

- This study shows clusters of Eu co-segregated with Al in eutectic Si matching the stoichiometry of  $\text{Al}_2\text{Si}_2\text{Eu}$  ternary compound. On the contrary, no Yb in the Si crystal was found. This result suggests that the existence of nanometre sized clusters of ternary compounds is a necessary condition for the formation of a coral-like structure.
- The formation of  $\text{Al}_2\text{Si}_2\text{Eu}$  and  $\text{Al}_2\text{Si}_2\text{Yb}$  during eutectic solidification proves the presence of a ternary eutectic reaction for these alloys.
- The parallel lattice plane-normals  $011_{\text{Si}}//0001_{\text{Al}_2\text{Si}_2\text{X}}$ ,  $011_{\text{Si}}//\bar{6}\bar{7}10_{\text{Al}_2\text{Si}_2\text{X}}$  and  $111_{\text{Si}}//\bar{6}\bar{7}10_{\text{Al}_2\text{Si}_2\text{X}}$  found only for the sample with Eu addition and not for Yb proves a favourable heterogeneous formation of  $\text{Al}_2\text{Si}_2\text{Eu}$  on Si. This explains the formation and adsorption of clusters of this phase in the alloy with Eu addition and not in the alloy with Yb addition.
- The misfit between  $011_{\text{Si}}$  and  $0002_{\text{Al}_2\text{Si}_2\text{X}}$  interplanar spacings shows a consistent trend with the potency of modification for several elements such as Sr, Na, Eu, Ca, Ba, Yb and Y.

In the present work, the growth restriction of eutectic Si by the formation of ternary clusters is proposed. The formation of such clusters on Si-facets creates growth steps increasing growth direction diversity. The incorporation of cluster onto the Si surface explains the high density of crystallographic defects in Si and the modification from Si plates to corals.

## Methods

Ingots of about 1 kg Al-5Si-0.05Eu and Al-5Si-0.61Yb alloys (wt. %) were produced by electric resistance melting of the charge material in a boron-nitride coated clay-graphite crucible at  $750^\circ\text{C}$  and then casted using gravity die casting. Prior to casting, no degassing treatment was performed. High purity Al (5N) and Si (5N) were used as starting materials. Master alloys, Al-2Eu and Al-5Yb, were used to add Eu and Yb when the starting materials (Al and Si) were fully molten. The modifier amounts were chosen to yield optimal modification based on previous studies<sup>22,24,29,31,53</sup>.

Microscopy samples were prepared from the casts by metal machining, followed by grinding and polishing to a mirror-like finish, where the last step was vibrational polishing in a colloidal silica suspension (Struers OP-S -  $0.04\mu\text{m}$ ) for 2 hours. TEM and APT samples were prepared in a dual-beam focused ion beam/scanning electron microscopy workstation (FIB/SEM) (Helios NanoLab 600<sup>TM</sup>, FEI Company, USA). APT specimen of the eutectic Si phase were prepared by the phase selective sample preparation method described in<sup>60</sup>. After lift out and thinning of the samples, a low energy milling at 2kV was performed to minimize gallium induced damage<sup>61</sup>.

An EDAX Hikari detector within the FIB/SEM workstation was used to record EBSD and TKD data using an electron beam of 20 kV/22 nA and 30 kV/5.5 nA, respectively.  $\text{Al}_2\text{Si}_2\text{Eu}$  and  $\text{Al}_2\text{Si}_2\text{Yb}$  crystal structures from literature<sup>32–34</sup> were added to OIM Data Collection 7 database by means of the built-in structure creation wizard. Post-processing of the data was performed using the OIM Analysis software (EDAX). Results are shown in the form of pole figures and inverse pole figure maps. In case of the TKD measurement shown in Fig. 5, a pseudosymmetry clean-up followed by a grain dilation was performed for visual representation. Pole figures were calculated from uncleaned data. Conventional EBSD scans in reflection mode yielded better pattern quality. Data points for pole figure calculation were extracted from uncleaned raw data using the grain highlight function of OIM Data Analysis software. This allows a point-and-click selection of data points belonging to a continuous grain based on a misorientation threshold (here  $5^\circ$ ). Data points from the intermetallic phase ( $\text{Al}_2\text{Si}_2\text{Eu}$  or  $\text{Al}_2\text{Si}_2\text{Yb}$ ) and the neighbouring Si phase were highlighted and used for the calculation of pole figures. No clean-up was used.

TEM and STEM imaging was performed in a Tecnai G2 TF 20 UT FEG (FEI) in micro and nanoprobe modes and a JEM - ARM 200 F Cold FEG TEM/STEM operating at 200kV and equipped with a spherical aberration (Cs) probe and image correctors (point resolution 0.12 nm in TEM mode and 0.078 nm in STEM mode).

APT was carried out in a LEAP 3000X HR (CAMECA) in laser mode to measure eutectic Si and voltage mode to measure eutectic Al. All measurements were performed at repetition rate of 200 kHz, pressure lower than  $1.33 \times 10^{-8}$  Pa, and evaporation rate of 5 atoms per 1000 pulses. Laser-pulsed APT was accomplished using a laser with a wavelength of 532 nm, pulse length of 10 ps, and a pulse energy of 0.3–0.4 nJ while keeping a specimen temperature of about 40 K. Voltage measurements were performed at 20% pulse fraction and a specimen temperature between 50 and 60 K. Datasets were reconstructed and analysed with IVAS<sup>TM</sup> 3.6.8 software (CAMECA). Al and Eu contents in Si were measured after background subtraction performed with IVAS software. The cleaning of the datasets for visualization purposes was performed with the open source software Blender 2.76 and the open access AtomBlend plugin developed by Peter Felner and Vavara Efremova<sup>62</sup>.



## Data Availability

The datasets analysed during the current study are available from the corresponding author on reasonable request.

## References

- Kaufman, J. G. & Rooy, E. L. *Aluminum Alloy Castings: Properties, Processes, and Applications* (ASM International, 2004).
- Samuel, A. M., Elgallad, E. M., Doty, H. W., Valtierra, S. & Samuel, F. H. Effect of metallurgical parameters on the microstructure, hardness impact properties, and fractography of Al-(6.5–11.5) wt% Si based alloys. *Mater. Des.* **107**, 426–439 (2016).
- Joseph, S. & Kumar, S. A systematic investigation of fracture mechanisms in Al-Si based eutectic alloy—Effect of Si modification. *Mater. Sci. Eng. A* **588**, 111–124 (2013).
- Gruzleski, J. E. & Closset, B. *The treatment of liquid Aluminum-Silicon alloys* (American Foundrymen Society, 1990).
- Samuel, A. M., Garza-Elizondo, G. H., Doty, H. W. & Samuel, F. H. Role of modification and melt thermal treatment processes on the microstructure and tensile properties of Al-Si alloys. *Mater. Des.* **80**, 99–108 (2015).
- Mohamed, A. M. A., Samuel, F. H., Samuel, A. M. & Doty, H. W. Influence of additives on the impact toughness of Al-10.8% Si near-eutectic cast alloys. *Mater. Des.* **30**, 4218–4229 (2009).
- Caceres, C. H. & Griffiths, J. R. Damage by the cracking of silicon particles in an Al-7Si-0.4Mg casting alloy. *Acta Mater.* **44**, 25–33 (1996).
- Riestra, M., Ghassemali, E., Bogdanoff, T. & Seifeddine, S. Interactive effects of grain refinement, eutectic modification and solidification rate on tensile properties of Al-10Si alloy. *Mater. Sci. Eng. A* **703**, 270–279 (2017).
- Jigajinni, S. M., Venkateswarlu, K. & Kori, S. A. Effect of a grain refiner cum modifier on mechanical properties of Al-7Si and Al-11Si alloys. *Met. Mater. Int.* **19**, 171–181 (2013).
- Tao, S., Pan, Y., Lu, T., Chen, Y. & Wu, J. Microstructures and mechanical properties of La added Al-Si casting alloys and mechanism of grain refinement. *Int. J. Cast Met. Res.* **28**, 375–381 (2015).
- Samuel, A. M., Doty, H. W., Valtierra, S. & Samuel, F. H. Effect of grain refining and Sr-modification interactions on the impact toughness of Al-Si-Mg cast alloys. *Mater. Des.* **56**, 264–273 (2014).
- Pacz, A. Alloy. U.S. Patent No. 1,387,900 (1921).
- McDonald, S. D., Dahle, A. K., Taylor, J. A. & StJohn, D. H. Eutectic grains in unmodified and strontium-modified hypoeutectic aluminum-silicon alloys. *Metall. Mater. Trans. A* **35**, 1829–1837 (2004).
- Dahle, A. K., Nogita, K., McDonald, S. D., Dinnis, C. & Lu, L. Eutectic modification and microstructure development in Al-Si Alloys. *Mater. Sci. Eng. A* **413–414**, 243–248 (2005).
- Cho, Y. H., Lee, H.-C., Oh, K. H. & Dahle, A. K. Effect of Strontium and Phosphorus on Eutectic Al-Si Nucleation and Formation of  $\beta$ -Al<sub>5</sub>FeSi in Hypoeutectic Al-Si Foundry Alloys. *Metall. Mater. Trans. A* **39**, 2435–2448 (2008).
- Flood, S. C. & Hunt, J. D. Modification of Al-Si eutectic alloys with Na. *Met. Sci.* **15**, 287–294 (1981).
- Kobayashi, K. F. & Hogan, L. M. The crystal growth of silicon in Al-Si alloys. *J. Mater. Sci.* **20**, 1961–1975 (1985).
- Shamsuzzoha, M. & Hogan, L. M. Twinning in fibrous eutectic silicon in modified Al-Si Alloys. *J. Cryst. Growth* **72**, 735–737 (1985).
- Lu, S. & Hellawell, A. The mechanism of silicon modification in aluminum-silicon alloys: Impurity induced twinning. *Metall. Trans. A* **18**, 1721–1733 (1987).
- Shamsuzzoha, M. & Hogan, L. M. The crystal morphology of fibrous silicon in strontium-modified Al-Si eutectic. *Philos. Mag. A* **54**, 459–477 (1986).
- Shamsuzzoha, M. & Hogan, L. M. The role of non-cozonal twinning in the growth of fibrous silicon in strontium-modified Al-Si eutectic. *J. Mater. Sci.* **24**, 2849–2859 (1989).
- Knuutinen, A., Nogita, K., McDonald, S. D. & Dahle, A. K. Modification of Al-Si alloys with Ba, Ca, Y and Yb. *J. Light Met.* **1**, 229–240 (2002).
- Ludwig, T. H., Schaffer, P. L. & Arnberg, L. Influence of Some Trace Elements on Solidification Path and Microstructure of Al-Si Foundry Alloys. *Metall. Mater. Trans. A* **44**, 3783–3796 (2013).
- Nogita, K., McDonald, S. D. & Dahle, A. K. Eutectic Modification of Al-Si Alloys with Rare Earth Metals. *Mater. Trans.* **45**, 323–326 (2004).
- Barrirero, J. *et al.* Comparison of segregations formed in unmodified and Sr-modified Al-Si alloys studied by atom probe tomography and transmission electron microscopy. *J. Alloys Compd.* **611**, 410–421 (2014).
- Barrirero, J. *et al.* Cluster formation at the Si/liquid interface in Sr and Na modified Al-Si alloys. *Scr. Mater.* **117**, 16–19 (2016).
- Li, J. H. H. *et al.* Nucleation and Growth of Eutectic Si in Al-Si Alloys with Na Addition. *Metall. Mater. Trans. A* **46**, 1300–1311 (2014).
- Timpel, M. *et al.* Sr-Al-Si co-segregated regions in eutectic Si phase of Sr-modified Al-10Si alloy. *Ultramicroscopy* **132**, 216–21 (2013).
- Li, J. *et al.* The roles of Eu during the growth of eutectic Si in Al-Si alloys. *Sci. Rep.* **5**, 13802 (2015).
- Nogita, K. *et al.* The role of trace element segregation in the eutectic modification of hypoeutectic Al-Si alloys. *J. Alloys Compd.* **489**, 415–420 (2010).
- Li, J. H., Suetsugu, S., Tsunekawa, Y. & Schumacher, P. Refinement of Eutectic Si Phase in Al-5Si Alloys with Yb Additions. *Metall. Mater. Trans. A* **44**, 669–681 (2012).
- Kranenberg, C. *et al.* Structure and properties of the compounds LnAl<sub>2</sub>X<sub>2</sub> (Ln = Eu, Yb; X = Si, Ge). *Solid State Sci.* **2**, 215–222 (2000).
- Bobev, S. *et al.* Ternary rare-earth aluminosilicides - Single-crystal growth from Al flux, structural and physical properties. *J. Solid State Chem.* **178**, 2091–2103 (2005).
- YbAl<sub>2</sub>Si<sub>2</sub> Crystal Structure: Datasheet from 'PAULING FILE Multinaries Edition - 2012' in Springer Materials ([https://materials.springer.com/isp/crystallographic/docs/sd\\_1210515](https://materials.springer.com/isp/crystallographic/docs/sd_1210515)).
- Lefebvre, W. *et al.* 3DAP measurements of Al content in different types of precipitates in aluminium alloys. *Surf. Interface Anal.* **39**, 206–212 (2007).
- Sha, G. *et al.* Solute nanostructures and their strengthening effects in Al-7Si-0.6Mg alloy F357. *Acta Mater.* **60**, 692–701 (2012).
- Gault, B. *et al.* Atom probe tomography and transmission electron microscopy characterisation of precipitation in an Al-Cu-Li-Mg-Ag alloy. *Ultramicroscopy* **111**, 683–9 (2011).
- Rüsing, J., Sebastian, J. T., Hellman, O. C. & Seidman, D. N. Three-dimensional Investigation of Ceramic/Metal Heterophase Interfaces by Atom-probe Microscopy. *Microsc. Microanal.* **6**, 445–451 (2000).
- Hasting, H. K. *et al.* Comparative study of the  $\beta''$ -phase in a 6xxx Al alloy by 3DAP and HRTEM. *Surf. Interface Anal.* **39**, 189–194 (2007).
- Dahle, A. K., Nogita, K., McDonald, S. D., Zindel, J. W. & Hogan, L. M. Eutectic nucleation and growth in hypoeutectic Al-Si alloys at different strontium levels. *Metall. Mater. Trans. A* **32**, 949–960 (2001).
- Zarif, M., McKay, B. & Schumacher, P. Study of Heterogeneous Nucleation of Eutectic Si in High-Purity Al-Si Alloys with Sr Addition. *Metall. Mater. Trans. A* **42**, 1684–1691 (2010).
- Li, J. H., Zarif, M. Z., Dehm, G. & Schumacher, P. Influence of impurity elements on the nucleation and growth of Si in high purity melt-spun Al-Si-based alloys. *Philos. Mag.* **92**, 3789–3805 (2012).

43. Ho, C. R. & Cantor, B. Modification of hypoeutectic Al-Si alloys. *J. Mater. Sci.* **30**, 1912–1920 (1995).
44. Ludwig, T. H., Schonhvd Dæhlen, E., Schaffer, P. L. & Arnberg, L. The effect of Ca and P interaction on the Al-Si eutectic in a hypoeutectic Al-Si alloy. *J. Alloys Compd.* **586**, 180–190 (2014).
45. Li, J. H. *et al.* Nucleation kinetics of entrained eutectic Si in Al-5Si alloys. *Acta Mater.* **72**, 80–98 (2014).
46. Eiken, J., Apel, M., Liang, S.-M. & Schmid-Fetzer, R. Impact of P and Sr on solidification sequence and morphology of hypoeutectic Al-Si alloys: Combined thermodynamic computation and phase-field simulation. *Acta Mater.* **98**, 152–163 (2015).
47. McDonald, S. D., Nogita, K. & Dahle, A. K. Eutectic nucleation in Al-Si alloys. *Acta Mater.* **52**, 4273–4280 (2004).
48. Day, M. G. & Hellawell, A. The Microstructure and Crystallography of Aluminium-Silicon Eutectic Alloys. *Proc. R. Soc. A Math. Phys. Eng. Sci.* **305**, 473–491 (1968).
49. Hellawell, A. The growth and structure of eutectics with silicon and germanium. *Prog. Mater. Sci.* **15**, 3–78 (1970).
50. Jenkinson, D. C. & Hogan, L. M. The modification of aluminium-silicon alloys with strontium. *J. Cryst. Growth* **28**, 171–187 (1975).
51. Hanna, M. D., Lu, S.-Z. & Hellawell, A. Modification in the aluminum silicon system. *Metall. Trans. A* **15**, 459–469 (1984).
52. Yilmaz, F., Atasoy, O. A. & Elliott, R. Growth structures in aluminium-silicon alloys II. The influence of strontium. *J. Cryst. Growth* **118**, 377–384 (1992).
53. Li, J. H. *et al.* Modification of eutectic Si in Al-Si alloys with Eu addition. *Acta Mater.* **84**, 153–163 (2015).
54. Ferro, R., Kubaschewski, O., Hubert, H. & Ibe, G. Aluminium-Silicon-Strontium. *VCH* **8**, 270–278 (1993).
55. Bochvar, N., Budberg, P., Hayes, F., Liberov, Y. & Schmid-Fetzer, R. *Al-Na-Si Ternary Phase Diagram* (MSI, Materials Science International Services GmbH, 1993).
56. Kumari, S. S. S., Pillai, R. M. & Pai, B. C. Role of calcium in aluminium based alloys and composites. *Int. Mater. Rev.* **50**, 216–238 (2005).
57. Davies, V. L. & West, J. M. Factors affecting the modification of the aluminium-silicon eutectic. *J. Inst. Met.* **92**, 175–180 (1963).
58. Steen, H. A. H. & Hellawell, A. The growth of eutectic silicon-contributions to undercooling. *Acta Metall.* **23**, 529–535 (1975).
59. Clapham, L. & Smith, R. W. Segregation behaviour of strontium in modified and unmodified Al-Si alloys. *J. Cryst. Growth* **92**, 263–270 (1988).
60. Barrirero, J., Engstler, M., Odén, M. & Mücklich, F. Phase selective sample preparation of Al-Si alloys for Atom Probe Tomography. *Pract. Metallogr.* **56**, 76–90 (2019).
61. Thompson, K. *et al.* *In situ* site-specific specimen preparation for atom probe tomography. *Ultramicroscopy* **107**, 131–9 (2007).
62. <https://github.com/annacegu/atomblend> - Accessed on 01.11.2018. 01.11.2018. Available at: <https://github.com/annacegu/atomblend> (Accessed: 1st November 2018).
63. Gladyshevskii, E. I., Kripyakevich, P. I. & Bodak, O. I. Crystal structure of  $\text{CaAl}_2\text{Si}_2$  and its analogs. *Ukr. Phys. J.* **12**, 447–452 (1967).
64. Westerhaus, W. & Schuster, H.-U. Darstellung und Struktur von  $\text{NaAlSi}$  und  $\text{NaAlGe}$ . *Tl. B Anorg. chemie, Org. chemie* **34B**, 352–353 (1979).
65. Yamanaka, S., Kajiyama, M., Sirakumar, S. N. & Fukuoka, H. Preparation and single crystal structure of a new high-pressure modification of  $\text{BaAl}_2\text{Si}_2$ . *High Press. Res.* **24**, 481–490 (2004).
66. Muraveva, A. A., Zarechnyuk, O. S. & Gladyshevskii, E. I. The systems Y-Al-Si(Ge,Sb) in the range 0–33.3 at.% Y. *Inorg. Mater.* **7**, 34 (1971).

## Acknowledgements

This work has been co-funded by the European Regional Development Fund (ERDF). The Atom Probe was financed by the DFG and the Federal State Government of Saarland (INST 256/298-1 FUGG). J. Barrirero acknowledges the Erasmus Mundus Programme of the European Commission within the Doctoral Programme DocMASE for financial support. J. Li gratefully acknowledges the financial support from the Major International (Regional) Joint Research Project (No. 51420105005) and the Overseas, Hong Kong, Macao Scholars Cooperative Research Fund (No. 51728101) from China. The authors want to thank the Australian Centre for Microscopy and Microanalysis for making the plugin AtomBlend for Blender available.

## Author Contributions

J.L. fabricated the samples. J.B. and M.E. performed SEM imaging and APT acquisition and analysis. C.P. and J.B. performed EBSD/TKD acquisition and analysis. J.G., N.G. and J.B. performed TEM acquisition and analysis. J.B. and M.O. wrote the first draft of the manuscript. J.B. prepared all images. All authors (J.B., C.P., M.E., J.G., N.G., J.L., P.S., M.O., F.M.) contributed substantially to the concepts, ideas and design of the experiments and to the discussion of the results. All authors reviewed and contributed to the manuscript.

## Additional Information

**Supplementary information** accompanies this paper at <https://doi.org/10.1038/s41598-019-41919-2>.

**Competing Interests:** The authors declare no competing interests.

**Publisher's note:** Springer Nature remains neutral with regard to jurisdictional claims in published maps and institutional affiliations.



**Open Access** This article is licensed under a Creative Commons Attribution 4.0 International License, which permits use, sharing, adaptation, distribution and reproduction in any medium or format, as long as you give appropriate credit to the original author(s) and the source, provide a link to the Creative Commons license, and indicate if changes were made. The images or other third party material in this article are included in the article's Creative Commons license, unless indicated otherwise in a credit line to the material. If material is not included in the article's Creative Commons license and your intended use is not permitted by statutory regulation or exceeds the permitted use, you will need to obtain permission directly from the copyright holder. To view a copy of this license, visit <http://creativecommons.org/licenses/by/4.0/>.

© The Author(s) 2019